Journal of Applied Science and Engineering, Vol. 22, No. 1, pp. 153–162 (2019) *DOI: 10.6180/jase.201903_22(1).0015*

Preparation of Nanosilica/polyacrylate Antifog Coatings on Polycarbonate Substrates

Chao-Chin Chang[1,2], Tsung-Ying Tsai[1] and Liao-Ping Cheng[1,2]*

[1]*Department of Chemical and Materials Engineering, Tamkang University, Tamsui, Taiwan 25137, R.O.C.*
[2]*Energy and Opto-Electronic Materials Research Center, Tamkang University, Tamsui, Taiwan 25137, R.O.C.*

Abstract

Superhydrophilic UV-curable nanosilica particles were synthesized through reaction of the surfactant, Tween-20, and the C=C containing silane, MSMA, with silica nanoparticles synthesized from hydrolysis and condensation of tetraethoxysilane in an acid catalyzed sol-gel process. The formed organic/inorganic hybrid nanoparticles were used to prepare antifog (AF) coatings with a special hydrophilic/hydrophobic bi-layer structure on polycarbonate (PC) substrates. The coatings were transparent, adhered strongly to the substrate, and demonstrated superb AF capability on steam tests. The hardness of the coatings reached 1H in the optimal case, considerably higher than that of the PC substrate (2B). After immersed in water for 24 h at 25 °C, this coating still demonstrated good AF capability; however, it took longer time (2 min) to retain transparency on the steam test.

Key Words: Anti-fogging, Silica, Nanocomposite, Coatings

1. Introduction

Fog forms when water molecules condense as discrete droplets large enough to scatter visible light and cause reduction of light transmittance. This phenomenon occurs frequently in our daily life and causes inconveniences. For example, fogs can form on eye-wears, swimming goggles, windshields of vehicles, and bathroom mirrors. Likewise, when forms on optical instruments and photoelectric devices, such as solar panels and infrared microscopes, fog may downgrade the efficiency and/or accuracy of that device. To avoid such undesirable occasions, it is operative to apply an antifog (AF) layer on the surface of use, particularly in case that the surface is hydrophobic and susceptible to moisture deposition [1–28].

Hydrophilic reagents (e.g., glycerol, poly(acrylic acid), poly(vinyl alcohol), surfactants, etc.) were often adopted to produce AF surfaces due to the fact that a hydrophilic surface can spread water droplets into a continuous film that allows transmission of visible lights. Many useful researches have been conducted on the basis of this principle [2–4,14–21]. For example, Maechler et al. prepared AF coatings with a poly(vinyl alcohol)/poly(ethylene-maelic anhydride)/Si-multilayer/PC configuration on polycarbonate (PC) substrates [19]. The Si-multilayer was strongly adhered to the substrate through chemical vapor deposition process. The poly(vinyl alcohol) (PVA) layer provided hydrophilicity, while the poly(ethylene-maelic anhydride) layer served as a covalent linker between PVA and Si-multilayer. The coating was found to resist fog formation upon cold-warm transition and humid air exposure. Zhang et al. partly crosslinked poly(acrylic acid) (PAA) with poly(vinyl alcohol) (PVA) on plasma-treated glasses or poly(ethylene terephthalate) (PET) substrates to form AF coatings [16]. With an appropriate adjustment of PAA/PVA ratio, the coating also demonstrated

*Corresponding author. E-mail: lpcheng@mail.tku.edu.tw

self-healing capability through reformation of hydrogen bonds. Howarter et al. prepared AF coatings by grafting the surfactant, perfluorinated polyethylene glycol oligomer (f-PEG), onto a glass surface pretreated with a silane-type coupling agent [5]. The coatings were dual-functional, as they exhibited hydrophilicity for AF and oleophobicity for contamination resistance.

Although many formulations and processes have been developed for preparing AF coatings for particular usages, it is surprising that the mechanical strengths of the coatings, e.g., hardness and adhesion, were rarely addressed in the literature. Previously, water-washable AF coatings with a bi-layer configuration were prepared in our laboratory [21]. The bottom layer (primer), serving as a binder and a mechanical support, is an inorganic-organic hybrid comprising silica and polyacrylate. The top layer was formulated based on the primer, while incorporating IPDI-and HEMA-modified Tween-20 as the hydrophilic agent. The coatings were very hard, adhere perfectly on the PMMA substrate, and performed well on steam tests. It is, however, found that the adherence and hardness (1B) of the coating became unsatisfactory, when the same formulation was applied on PC substrates (hardness 2B). Thus, in this research, a new formulation was designed with the aim to improve the adhesion strength and hardness of the AF coatings on the soft PC substrates. The detailed preparation procedure and characterizations are introduced in the sections that follow.

2. Methods

2.1 Material

3-(Trimethoxysilyl) propyl methacrylate (MSMA, 98%), tetraethoxysilane (TEOS, > 98%), 2-hydroxyethyl methacrylate (2-HEMA, 97%), polyoxyethylene (20) sorbitan monolaurate (Tween-20, Mw = 1227.5), 2-propanol (IPA, 99.8%), and dipentaerythritol hexaacrylate (DPHA, regent grade) were purchased from Aldrich. Methyl ethyl ketone (MEK, 99.5%) was purchased from J.T. Baker. 1,6-Hexanediol diacrylate (HDDA, 97%) was provided by Eternal Chemical, Taiwan. The photo initiator, 2-hydroxy-2-methyl-hexanediol-1-phenyl-propan-1-one (Darocure 1173, 99.8%) was supplied by Ciba-Geigy Ltd. All materials were used as received.

2.2 Preparation of the Anti-fog Coatings

2.2.1 The Bottom Layer (primer)

The UV-curable coating sol for the primer was prepared by mixing the monomers (DPHA, HDDA, and 2-HEMA), photo-initiator (Darocure 1173), and the solvent (MEK) at room temperature in a dark bottle. The molar ratio of HDDA/DPHA/2-HEMA was 2.2/9/1. The amount of Darocure 1173 accounted for 5% of the total weight of added monomers. The solid content was adjusted to 50% by means of MEK. The obtained sol was roller-coated (50 μm) on a PC substrate, and then pre-baked at 80 °C for 30 s., followed by UV-irradiation to yield a cured film on the substrate. The irradiation power was carefully chosen such that DPHA was only partly cross-linked (~60% according to the FTIR spectroscopy). The remaining double bonds can be used to link with the top (AF) layer during subsequent UV-curing.

2.2.2 The Top Layer

Firstly, the surfactant, Tween-20, was modified by reaction with the NCO-containing silane, ICPTES (cf. Scheme 1). ICPTES and Tween-20 at the molar ratio of 1:2 were mixed with dehydrated MEK (molar ratio of Tween-20:MEK = 1:23.6) at room temperature for the period of 30 min. under de-aeration ($N_{2(g)}$). Then, the temperature was raised to 50 °C, and dibutyltin dilaurate (0.2% of the total weight of ICPTES and Tween-20) acting as the catalyst was added to invoke the urethanation reaction, which was allowed to proceed for 5 h. Periodically, aliquots of samples were withdrawn and FTIR-analyzed to monitor the progress of the reaction. The ob-

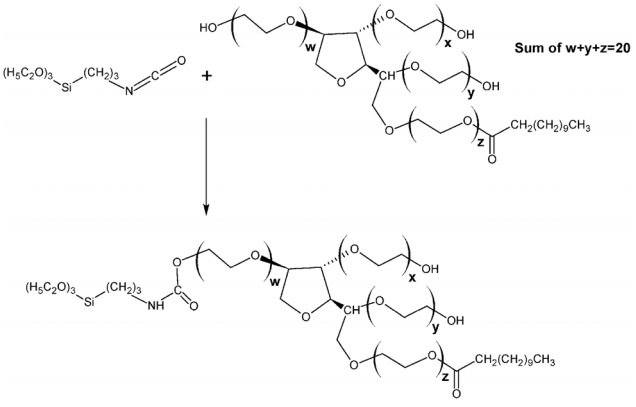

Scheme 1. Synthetic route for the hydrophilic agent, T20.

tained hydrophilic agent (ICPTES-Tween20) is abbreviated as T20, hereinafter.

Then, the formed T20 was bonded to silica nanoparticles by a modified sol-gel process, cf. Scheme 2(a) and 2(b). Briefly, an appropriate amount of TEOS was mixed with 2-propanol (weight ratio of TEOS/IPA = 4.5/5.0) to form a homogeneous solution. Thereafter, $HCl_{(aq)}$ (pH 1.2) was added to trigger the hydrolysis and condensation of TEOS. The molar ratio of H_2O/TEOS was set to 4, and the reaction was continued for 3 h under agitation. Silica nanoparticles of ~3 nm were formed during this period, as determined by dynamic light scattering method. Then, T20 solution was slowly added in the sol together with an additional amount of $HCl_{(aq)}$. The weight ratio of T20 solution/silica sol/$HCl_{(aq)}$ was 70/88/10.8. After 3 h of reaction, the coupling agent, MSMA, and additional $HCl_{(aq)}$ were added drop-by-drop into the silica sol, cf. Scheme 2(c). The reaction was carried out for another 3 h to yield modified nano-silica particles (termed $MTSiO_2$) that contained both C=C and Tween-20 on their surfaces. The compositions of various species for this reaction are summarized in Table 1. The top AF layer was prepared by adding appropriate amount of photo-initiator to the as-prepared sol, roller-coating it on the partly-cured bottom layer, followed by pre-drying (80 °C, 30 s) and UV-curing to give a film of ca. 15 μm in thickness. The formed AF coatings were heat treated at 80 °C for 2 h to remove residual solvents.

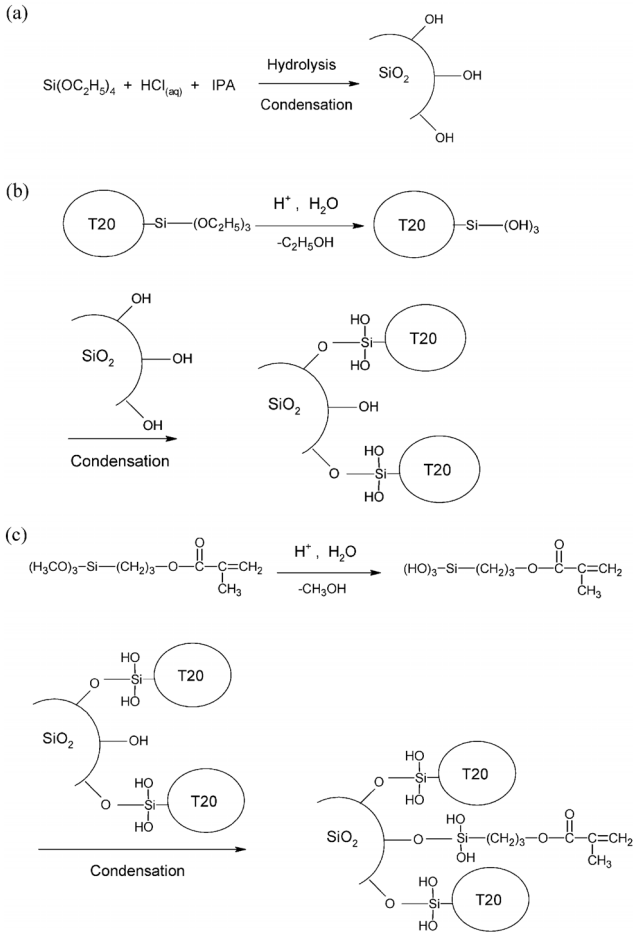

Scheme 2. Synthetic pathways of chemical species used for preparing AF coatings: (a) Silica; (b) $TSiO_2$; (c) $MTSiO_2$.

2.3 Characterization

The synthesized sols and the AF coatings were characterized by the following methods:

(1) The infrared absorption spectra of the samples were recorded on a Fourier transform infrared spectrophotometer (FTIR, Nicolet spectrometer 550, USA). For sols, the sample was dropped onto a KBr disc, and then the solvent was removed by evaporation under vacuum. For cured films, spectra were obtained in the attenuated total reflection (ATR) mode. For all experimental runs, spectra were collected over the wavenumber range of 400-4000 cm-1 with a resolution of 4 cm-1.

(2) Nuclear magnetic resonance (^{1}H-NMR) spectrometry was employed to confirm successful synthesis of T-20. The spectra were recorded on an NMR spectrometer (Avance AVII 600, Bruker, Germany) operated at 600 MHz with deuterated acetone used as the locking solvent (chemical shift, δ~2.1 ppm).

(3) The size and size distribution of nano-silica dispersed in the sol were determined using a particle sizer that applies dynamic light scattering protocol (Malvern,

Table 1. Compositions of various species for preparing $MTSiO_2$

Sample code	T20 sol (g)	SiO_2 sol (g)	$HCl_{(aq)}$ (g)			MSMA (g)
			(1)[a]	(2)[b]	(3)[c]	
T2S1	70	88	17.9	10.8	2.16	9.92
T2S2	70	88	17.9	10.8	3.24	14.88
T2S3	70	88	17.9	10.8	6.48	29.76
T0S1	70	–	17.9	10.8	2.16	9.92
T0S2	70	–	17.9	10.8	3.24	14.88
T0S3	70	–	17.9	10.8	6.48	29.76

[a]: scheme 2(a); [b]: scheme 2(b); [c]: scheme 2(c).

Zetasizer-3000 HS). The instrument incorporates a monochromatic coherent helium neon laser (633 nm) as the light source. A 4 ml sample was injected into the quartz cuvette secured on the holder, and then the scattered light was recorded at an angle of 173° with respect to the incident beam.

(4) Morphologies of the cured films were observed using field emission scanning electron microscope (Leo 1530 FE-SEM, Carl Zeiss). The sample was vacuum-dried and then coated with a layer (ca. 1.0 nm) of a Pt-Pd alloy by means of a sputter coater equipped with a quartz crystal microbalance (QCM) thickness controller. Then, it was imaged at high magnifications (e.g., 100 KX) under the acceleration voltage of 2.5 kV via an in-lens detector.

(5) The contact angle of water on an AF surface was assessed by a contact angle/surface tension analyzer (FTA 125, First Ten Angstroms) at 25 °C. A 6 μl drop of water was deposited onto the AF surface. The obtained image was shape-analyzed to give the contact angle. For each sample, measurement was taken at five different locations and the average value was reported.

(6) Light transmittances of the coatings were measured using a UV/Vis spectrometer (UV 500, Unicam) over the wavelength range of 350-800 nm. The intensity of the transmitted light was collected and converted to transmittance by the built-in software.

(7) Steam tests of various coatings were performed to see their AF capability [21]. The coating surface was exposed to saturated vapor of water at ~95 °C. Condensation of water droplets occurring on the surface was photographed.

(8) Tape tests (ASTM D3359), also known as the peel test, were performed to evaluate the adhesion strength of the coatings. The degree of adhesion (percentage of film resided on the substrate) was counted after being peeled by standard tapes (3M-610). The hardness of the coatings was examined by the widely used pencil test (ASTM D3359) using pencils (JIS K5400, Mitsubishi) of different hardness at the load of 750 g.

3. Results and Discussion

3.1 Chemical Analyses

The FTIR spectra at different times during synthesis T20 (cf., Scheme 1) is shown in Figure 1. The absorption at 2276 cm^{-1} corresponds to the vibrations of –NCO groups of ICPTES, which is absent from the spectrum of pure Tween-20 [21]. The band at 1735 cm^{-1} stands for the stretching vibration of C=O groups on ICPTES or Tween-20. The –OH signal of Tween-20, can be found as a broad hump around 3500 cm^{-1}. Along the progress of the reaction, the –NCO signal declines and a new band at 1536 cm^{-1} (assigned to –NH absorption) emerges and grows, which proves the formation of urethane linkage between Tween-20 and ICPTES. After 5 h of reaction, the –NCO signal vanishes and –NH reaches its maximum level. That is, the reaction is completed at this time. It is noted that the –SiOC bands at 1103 and 1079 cm^{-1} remained unchanged throughout the synthesis process. Hence, the silane groups could be used in subsequent sol-gel procedures to form $MTSiO_2$ nanoparticles, c.f. Scheme 2.

The NMR spectrum T20 synthesized with an ICPTES: Tween-20 molar ratio of 2:1 is shown in Figure 2. The five characteristic peaks (δ = 3.1 (a), 1.7 (b), 0.7 (c), 3.9 (d), and 1.2 (e) ppm) of the ICPTES moiety can be identified, which correspond to the resonance of hydrogen in (=N)CH_2(CH_2-), (-CH_2)CH_2(CH_2-), (CH_2-)CH_2(Si-), (-Si)(O)CH_2-, and (-O)(CH_2-)CH_3 groups [29]. For the Tween-20 part, the chemical shifts at δ = 0.9, 1.3, 1.6, 2.3, 3.6, and 4.1 ppm depict the resonances of CH_3, $(CH_2)_n$, $CH_2(CH_2)$(C=O), $(CH_2)CH_2$(C=O), $(CH_2\ CH_2O)_n$, and $O{=}COCH_2$, respectively [30]. The synthesized T20

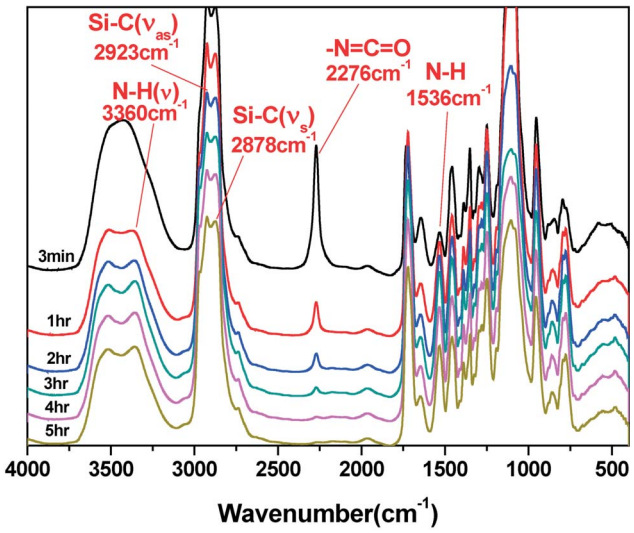

Figure 1. FTIR spectra of the modified Tween-20 (T20) at different times during synthesis.

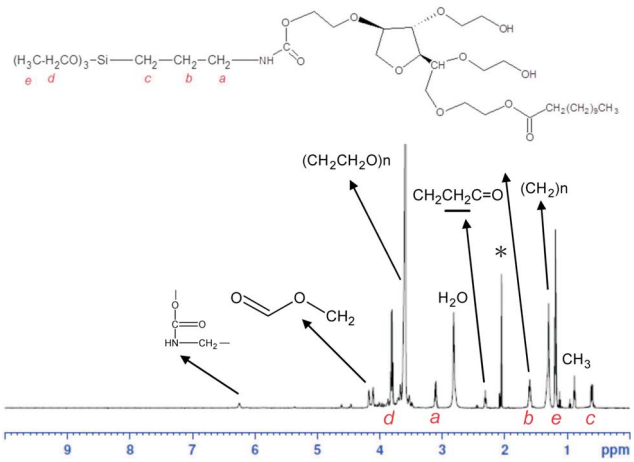

Figure 2. NMR spectra of T20 synthesized from 2:1 molar ratio of ICPTES and Tween-20.

exhibits a new chemical shift at 6.2 ppm, which stems from the –NH on the urethane bond of T20 [30]. Also noted is the change of peak "*a*" (3.4 ppm) in pure ICPTES (CH_2N=C=O) to 3.1 pm in T20 (CH_2NHC=O). These evidences assure urethane linkage being successfully formed via reaction between ICPTES and Tween-20.

Silica nanoparticles were synthesized by hydrolysis and condensation of TEOS in the presence of $HCl_{(aq)}$, cf. Scheme 2(a). FTIR analysis for this reaction can be found in the literature [31–35]. The formed silica was then reacted with T20 to give hydrophilic nanoparticles ($TSiO_2$), cf. Scheme 2(b). The reaction was examined by FTIR and the obtained spectra are shown in Figure 3. The absorptions at 1100, 785, and 434 cm^{-1} correspond to the asymmetric stretching, symmetric stretching, and bending vibrations of Si-O-Si, respectively. The Si-OH signals can be found at 950 cm^{-1} (symmetric stretching) and 3333 cm^{-1} (asymmetric stretching). The intensities of these absorptions increase during the course of reaction. The C=O at 1698 cm^{-1} and CH_3 at 2923 cm^{-1} signify the presence of T20 on $TSiO_2$ nanoparticles. $TSiO_2$ was further modified by bonding with MSMA, cf. Scheme 2(c). FTIR spectra related to this reaction and UV-curing of the C=C on $MTSiO_2$ nanoparticles have been presented previously [32–35].

3.2 DLS Analysis, SEM Imaging, and Transmittance

Dynamic light scattering (DLS) was used to determine the size of $MTSiO_2$ particles dispersed in the sol. For sample T2S2, Figure 4(a) shows that the particle size falls over a small range of 2-12 nm. The maximum number percentage occurs at 3.2 nm and most of the particles are smaller than 5 nm, which implies that particle-particle aggregation is not in evidence in the present case. Such is typical of sol-gel processes carried out under strong acidic conditions. Figure 4(b) shows the average size of nanoparticles (i.e., SiO_2, $TSiO_2$, and $MTSiO_2$) at different times during their synthetic process, c.f., Scheme 2. The particles grow very rapidly after initiation due to condensation between Si-OH groups of silica, then the growth rate declines, and after ca. 1 h of reaction the particles gradually approach a final average size of 3.2 nm. As these nanoparticles contain C=C double bonds on their surface, it is possible to chemically link them to the polymer matrix through UV-curing.

Figure 5 shows the cross sectional SEM micrographs of the cured coating T2S2. At a lower magnification, Figure 5(a) indicates that the cross section comprises two continuous layers with thickness being 9.1 for the primer and 6.53 μm for the AF layer. The total thickness (~16 μm) is consistent with that measured by a thickness gauge (BYK), 14 ± 2 μm. The high magnification image of a typical region in the AF layer is illustrated in Figure 5(b). It is uniform free of any aggregated or phase-separated domains under the resolvable length scale of 30 nm. That is, $MTSiO_2$ particles have been finely dispersed in the polymer matrix through covalent linkages between the organic moiety of $MTSiO_2$ and the polymer.

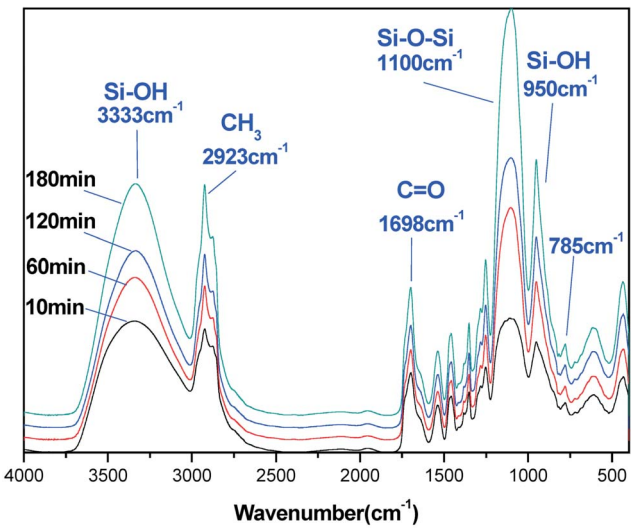

Figure 3. FTIR spectra at different times during synthesis of T20-modified silica, $TSiO_2$.

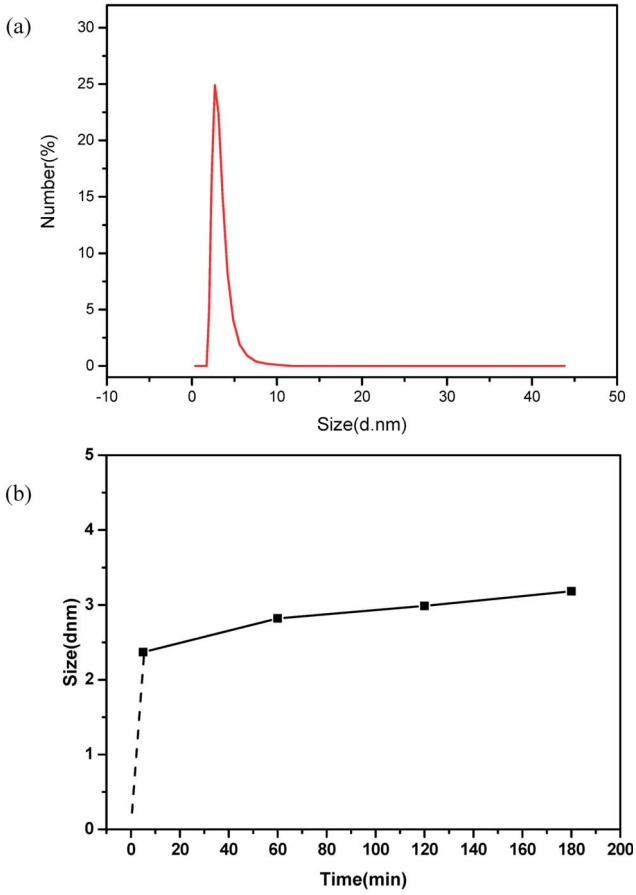

Figure 4. Particle size of $MTSiO_2$ determined by dynamic light scattering: (a) distribution of particle size in the sample T2S2; (b) growth of particle size during synthesis of T2S2. Dotted line is drawn for comparison of the growth rate.

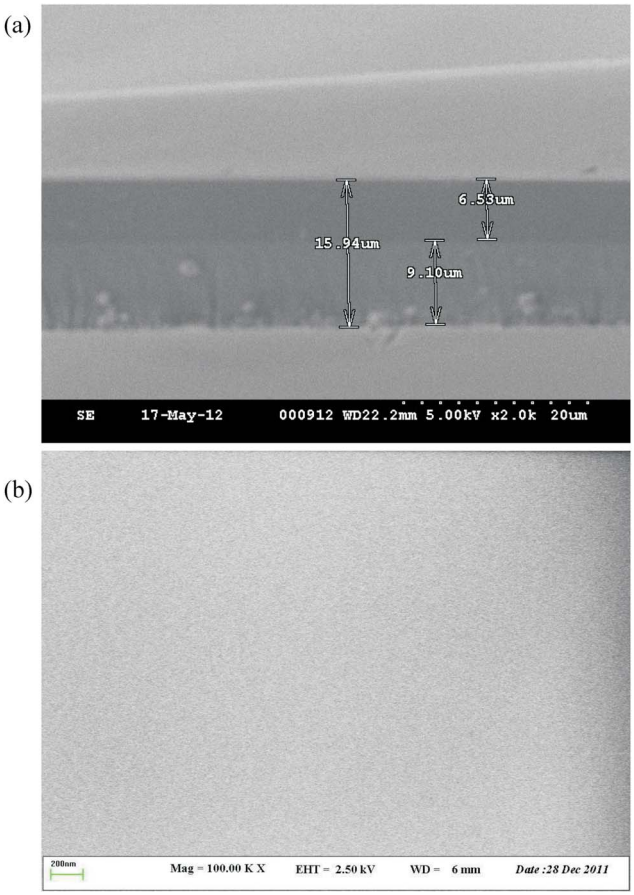

Figure 5. Cross sectional SEM images of the coating T2S2: (a) total cross section; (b) high magnification of a randomly chosen region in the top AF layer.

Light transmittance of the coatings confirms the SEM observation. As shown in Figure 6(a), all of the tested samples are transparent with transmittance approaching that of the PC substrate (~92%). The sample T2S2 was soaked in water (25 °C) for 24 h, dried under ambient condition, and then its transmittance again measured. Figure 6(b) indicates that even after soaking, the transmittance remains virtually unchanged; in other words, the coating tolerates well plain water-washing.

3.3 Contact Angle, Mechanical Strength, and AF Performance

Contact angle, hardness, adhesion strength, and AF performance of the coatings were examined and the results are summarized in Table 2. The PC substrate is quite soft with a measured pencil hardness of 2B only. And because it is hydrophobic (water contact angle = 70°), fogs form quickly on the exposed surface during a steam test, cf., Figure 7(a). After coated with a layer of primer, the hardness increases considerably to 2H and the contact angle drops to 40°. Obviously, the hexa-functional monomer DPHA has been converted to a strong crosslinked network, which imparts protections against mechanical impacts exerted by the pencil. Meanwhile, the 2-HEMA groups in the primer enhance hydrophilicity and bring down the water contact angle. Peel tests indicates that the primer adheres strongly (5B) onto the PC substrate without any trace of detachments. Thus, the present primer formulation works appropriately in terms of mechanical strength and adherence.

Application of an AF layer on the primer brings in super-hydrophilicity. In this case, the contact angles of the coatings become effectively zero degree, cf. Table 2.

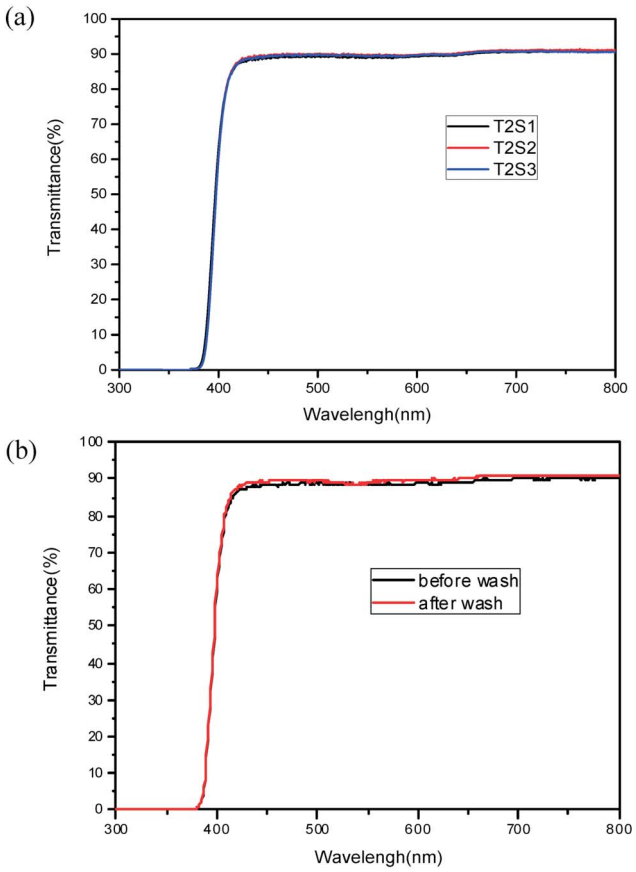

Figure 6. Transmittance of the anti-fog coatings. (a) T2S1, T2S2, and T2S3; (b) T2S2 before and after soaking in water at 25 °C for 24 h.

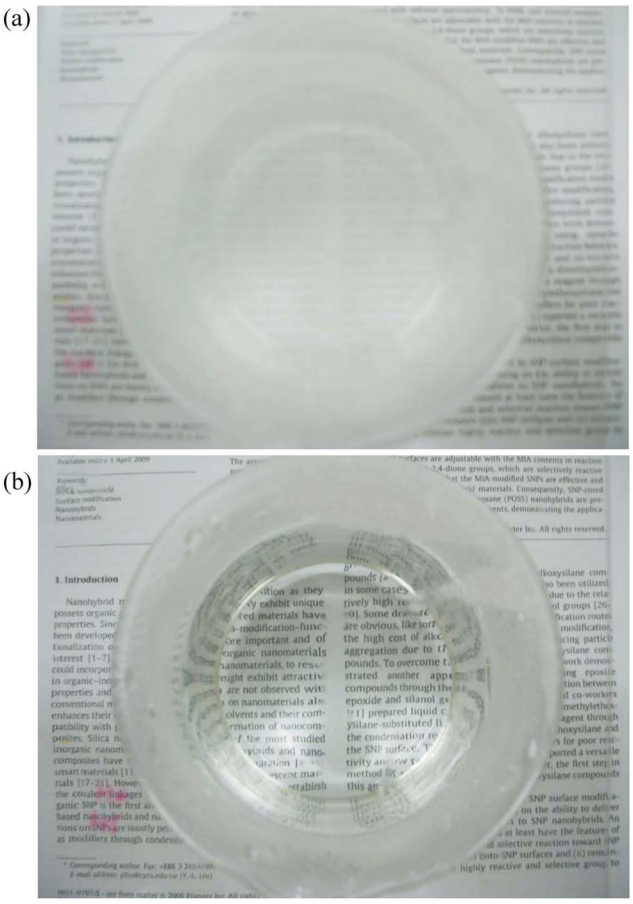

Figure 7. AF performance of the substrate and AF coating, as examined by steam tests. (a) PC substrate; (b) sample T2S1.

Table 2. Contact angle, hardness/adhesion, and AF performance of the coatings

Sample code	Hardness[a] (H)	Adherence	Contact angle (degree)	Transmittance[b] (%)	Steam test
PC	2B	-	70	92	foggy
Primer	2H	5B*	40	92	foggy
T2S1	HB	5B	0	90	transparent
T2S2	H	5B	0	88	transparent
T2S3	H	5B	0	87	transparent
T0S1	B	5B	0	90	transparent
T0S2	HB	5B	0	86	transparent
T0S3	HB	5B	0	90	transparent

* 5B = 100%.

As a result, water droplets will spread spontaneously as soon as they touch the surface. The AF capability of one such coating (T2S1) in the steam test is demonstrated in Figure 7(b). It can be seen that the English letters underneath the AF-treated area are well-defined; however, they are invisible for the untreated area. The hardness of the AF layer depends on the formulations, particularly, the SiO_2 and MSMA contents. For example, the hardness of T0S1 is only 1B due to the absence of SiO_2 sol in its synthesis. Incorporation of silica nanoparticles strengthens

the coating considerably. In the cases of T2S1 and T2S2, the hardness reaches HB and 1H, respectively. Enhancement of hardness by MSMA is evident from comparison of the hardness data of T0S1 (B) with T0S3 (HB) or T2S1 (HB) with T2S2 (H). Such is because MSMA not only provides silanol groups for bonding with silica nanoparticles, but also C=C groups for crosslinking with the rigid primer. The AF capability of the coating T2S1 after being soaked in water for 24 h. at 25 °C was examined. Fogs formed on the surface at first, and then after ~2 min of standing, fogs disappeared and the surface turned transparent once again. That is, soaking has downgraded the AF capability of the coating. It is though that some unbounded hydrophilic species have left the AF layer and migrated into the water bath during the soaking process. Therefore, the present AF coatings is more suited to applications where severe washing is not mandatory, such as those used on windshield or back mirror of a vehicle.

4. Conclusion

Anti-fog coatings with a hydrophilic/hydrophobic bi-layer configuration were prepared on polycarbonate (PC) substrates. The upper layer was an organic/inorganic silica hybrid ($MTSiO_2$) containing Tween-20 and C=C moieties, and was synthesized through a modified sol-gel method at 25 °C. Tween-20 in this layer provided hydrophilicity while C=C was used to chemically linked with the lower layer (primer), which comprised UV-curable monomers, including DPHA, 2-HEMA and HDDA. The formed coatings were highly transparent (transmittance ~90%), adhered perfectly (5B) to PC, extremely hydrophilic (contact angle ~0°), and demonstrated superb AF capability in the steam tests. Through crosslinking of multi-functional monomers in the primer, hardness of the coating reached 1H (vs. 2B for PC) in the optimal case. After soaking in water for 24 h, this coating still demonstrated AF capability; however, it took 2 min to totally spread the deposited water molecules into a transparent film in the steam test.

Acknowledgement

The authors thank the ministry of science and technology of Taiwan for financial support (MOST: 104-2221-E-032-053-MY2).

References

[1] Aegerter, M. A., R. Almeida, A. Soutar, K. Tadanaga, and H. Yang (2008) Coatings made by sol-gel and chemical nanotechnology, *Journal of Sol-Gel Science and Technology* 47(2), 203–236. doi: 10.1007/s10971-008-1761-9

[2] Feng, X., and L. Jiang (2006) Design and creation of superwetting/antiwetting surfaces, *Advanced Materials* 18(23), 3036–3078. doi: 10.1002/adma.200501961

[3] Drelich, J., E. Chibowski, D. D. Meng, and K. Terpilowskic (2011) Hydrophilic and superhydrophilic surfaces and materials, *Soft Matter* 7(21), 9804–9828. doi: 10.1039/C1SM05849E

[4] Howarter, J. A., and J. P. Youngblood (2007) Self-cleaning and anti-fog surfaces via stimuli-responsive polymer brushes, *Advanced Materials* 19(22), 3838–3843. doi: 10.1002/adma.200700156

[5] Howarter, J. A., and J. P. Youngblood (2008) Self-cleaning and next generation anti-fog surfaces and coatings, *Macromolecular Rapid Communications* 29(6), 455–466. doi: 10.1002/marc.200700733

[6] Nuraje, N., R. Asmatulu, R. E. Cohen, and M. F. Rubner (2011) Durable antifog films from layer-by-layer molecularly blended hydrophilic polysaccharides, *Langmuir* 27(2), 782–791. doi: 10.1021/la103754a

[7] Dong, H., P. Ye, M. Zhong, J. Pietrasil, R. Drumright, and K. Matyjaszewski (2010) Superhydrophilic surfaces via polymer-SiO_2 nanocomposites, *Langmuir* 26(19), 15567–15573. doi: 10.1021/la102145s

[8] Leonard, R. L., A. Y. Terekhov, C. Thompson, R. A. Erck, and J. A. Johnson (2012) Antifog coating for bronchoscope lens, *Surface Engineering* 28(6), 468–472. doi: 10.1179/1743294412Y.0000000007

[9] Wang, S., K. Liu, X. Yao, and L. Jiang (2015) Bioinspired surfaces with superwettability: New insight on theory, design, and applications, *Chemical Review* 115(16), 8230–8293. doi: 10.1021/cr400083y

[10] Kim, P., T. S. Wong, J. Alvarenga, M. J. Kreder, W. E. Adorno-Martinez, and J. Aizenberg (2012) Liquid-infused nanostructured surfaces with extreme anti-ice and anti-frost Performance, *ACS Nano* 6(8), 6569–

6577. doi: 10.1021/nn302310q

[11] Tahk, D., T. Kim, H. Yoon, M. Choi, K. Shin, and K. Y. Suh (2010) Fabrication of antireflection and antifogging polymer sheet by partial photopolymerization and dry etching, *Langmuir* 26(4), 2240–2243. doi: 10.1021/la904768e

[12] Li, X., and J. He (2012) In situ assembly of raspberry- and mulberry-like silica nanospheres toward antireflective and antifogging coatings, *ACS Applied Materials & Interfaces* 4(4), 2204–2211. doi: 10.1021/am3002082

[13] Lee, H., M. L. Alcaraz, M. F. Rubner, and R. E. Cohen (2013) Zwitter-wettability and antifogging coatings with frost-resisting capabilities, *ACS Nano* 7(3), 2172–2185. doi: 10.1021/nn3057966

[14] Wang, Y., Y. Li, S. Li, and J. Sun (2015) Antifogging and frost-resisting polyelectrolyte coatings capable of healing scratches and restoring transparency, *Chemistry of Materials* 27(23), 8058–8065. doi: 10.1021/acs.chemmater.5b03705

[15] Zhao, J., A. Meyer, L. Ma, and W. Ming (2013) Acrylic coatings with surprising antifogging and frost-resisting properties, *Chemical Communications* 49(100), 11764–11764. doi: 10.1039/c3cc46561f

[16] Zhang, X., and J. He (2015) Hydrogen-bonding-supported self-healing antifogging thin films, *Scientific Reports* 5, 9227. doi: 10.1038/srep09227

[17] Yuan, Y., R. Liu, C. Wang, J. Luo, and X. Liu (2014) Synthesis of UV-curable acrylate polymer containing sulfonic groups for anti-fog coatings, *Progress in Organic Coatings* 77(4), 785–789. doi: 10.1016/j.porgcoat.2014.01.001

[18] Shibraen, M. H. M. A., H. Yagoub, X. Zhang, J. Xu, and S. Yang (2016) Anti-fogging and anti-frosting behaviors of layer-by-layer assembled cellulose derivative thin film, *Applied Surface Science* 370, 1– 5. doi: 10.1016/j.apsusc.2016.02.060

[19] Maechler, L., C. Sarra-Bournet, P. Chevallier, N. Gherardi, and G. Laroche (2011) Anti-fog layer deposition onto polymer materials: a multi-step approach, *Plasma Chemistry and Plasma Processing* 31(1), 175–187. doi: 10.1007/s11090-010-9261-4

[20] Plasman, V., T. Caulier, and N. Boulos (2005) Polyglycerol esters demonstrate superior antifogging properties for films, *Plastics Additives & Compounding* 7(2), 30–33. doi: 10.1016/S1464-391X(05)00359-4

[21] Chang, C. C., F. H. Huang, H. H. Chang, T. M. Don, C. C. Chen, and L. P. Cheng (2012) Preparation of water-resistant antifog hard coatings on plastic substrate, *Langmuir* 28(49), 17193–17201. doi: 10.1021/la304176k

[22] Oguri, K., N. Iwataka, A. Tonegawa, Y. Hirose, K. Takayama, and Y. Nishi (2001) Misting-free diamond surface created by sheet electron beam irradiation, *Journal of Materials Research* 16(2), 553–557. doi: 10.1557/JMR.2001.0079

[23] Briscof, B. J., and K. P. Galvin (1991) The effect of surface fog on the transmittance of light, *Solar Energy* 46(4), 191–197. doi: 10.1016/0038-092X(91)90063-3

[24] Zhao, H., and D. Beysens (1995) From droplet growth to film growth on a heterogeneous surface - condensation associated with a wettability gradient, *Langmuir* 11(2), 627–634. doi: 10.1021/la00002a045

[25] Gao, X. F., X. Yan, X. Yao, L. Xu, K. Zhang, J. H. Zhang, B. Yang, and L. Jiang (2007) The dry-style antifogging properties of mosquito compound eyes and artificial analogues prepared by soft lithography, *Advanced Materials* 19, 2213–2217. doi: 10.1002/adma.200601946

[26] Cebeci, F. C., Z. Z. Wu, L. Zhai, R. E. Cohen, and M. F. Rubner (2006) Nanoporosity-driven superhydrophilicity: a means to create multifunctional antifogging coatings, *Langmuir* 22(6), 2856–2862. doi: 10.1021/la053182p

[27] Machida, M., K. Norimoto, T. Watanabe, K. Hashimoto, and A. Fujishima (1999) The effect of SiO2 addition in super-hydrophilic property of TiO2 photocatalyst, *Journal of Materials Science* 34(11), 2569–2574. doi: 10.1023/A:1004644514653

[28] Chang, C. C., K. C. Wang, C. C. Chen, and L. P. Cheng (2014) Preparation and characterization of silica/ polymer antifogging coatings, *Polymers and Polymer Composites* 22(1), 39–44.

[29] Cui, Y., M. Wang, L. Chen, and G. Qian (2005) Synthesis and characterization of an alkoxysilane dye for nonlinear optical applications, *Dyes and Pigments* 65(1), 61–66. doi: 10.1016/j.dyepig.2004.07.002

[30] Verbrugghe, M., P. Sabatino, E. Cocquyt, P. Saveyn, D. Sinnaeve, P. Van der Meeren, and J. C. Martins (2010) Solubilization of flurbiprofen with non-ionic Tween20 surfactant micelles: a diffusion 1H NMR

study, *Colloids and Surfaces A: Physicochemical and Engineering Aspects* 372(1), 28–34. doi: 10.1016/j.colsurfa.2010.09.020

[31] Yu, Y. Y., C. Y. Chen, and W. C. Chen (2003) Synthesis and characterization of organic-inorganic hybrid thin films from poly(acrylic) and monodispersed colloidal silica, *Polymer* 44(3), 593–601. doi: 10.1016/S0032-3861(02)00824-8

[32] Chen, C. C., D. J. Lin, T. M. Don, F. H. Huang, and L. P. Cheng (2008) Preparation of organic-inorganic nanocomposites for antireflection coatings, *Journal of Non-crystalline Solid* 35(32), 3828–3835. doi: 10.1016/j.jnoncrysol.2008.04.010

[33] Chang, C. C., T. Y. Oyang, Y. C. Chen, F. H. Hwang, and L. P. Cheng (2014) Preparation of hydrophobic nanosilica filled polyacrylate hard coatings on plastic substrates, *Journal of Coatings Technology and Research* 11(3), 381–386. doi: 10.1007/s11998-013-9540-0

[34] Chang, C. C., Z. M. Lin, S. H. Huang, and L. P. Cheng (2015) Preparation of highly transparent 13F-modified nano-silica/polymer hydrophobic hard coatings on plastic substrates, *Journal of Applied Science and Engineering* 18(4), 387–394. doi: 10.6180/jase.2015.18.4.10

[35] Chang, C. C., J. H. Lin, and L. P. Cheng (2016) Preparation of solvent-dispersible nano-silica powder by sol-gel method, *Journal of Applied Science and Engineering* 19(4), 401–408. doi: 10.6180/jase.2016.19.4.03

Manuscript Received: May 31, 2018
Accepted: Oct. 2, 2018